Petroleum 8 (2022) 318–331

Contents lists available at ScienceDirect

Petroleum

journal homepage: www.keaipublishing.com/en/journals/petlm

A new integrated approach to resolve the saturation profile using high-resolution facies in heterogenous reservoirs

Abdelrahman Elkhateeb [a, *], Reza Rezaee [a], Ali Kadkhodaie [b]

[a] WA School of Mines: Minerals, Energy and Chemical Engineering, Curtin University, Perth, Australia
[b] Earth Sciences Department, Faculty of Natural Sciences, University of Tabriz, Tabriz, Iran

ARTICLE INFO

Article history:
Received 10 January 2021
Received in revised form
2 June 2021
Accepted 23 June 2021

Keywords:
Reservoir facies
Permeability
Hydraulic flow units
Formation evaluation
Shaly sand
Saturation height modeling

ABSTRACT

The saturation calculation in complex reservoirs remains a major challenge to the oil and gas industry. In simple formations, a tendency towards simple saturation models such as Archie or Simandoux for clean and shaly reservoirs respectively is always preferable. These models were found to be working effectively in homogeneous formations within which the porosity and permeability are linked in the light of a simple facies scheme. Where the rocks show some degrees of heterogeneity, the well-logs are usually affected by different factors. This adversely results in a compromised or averaged log profiles that may affect the saturation calculations. Four wells drilled across a shaly sand of high heterogeneity have been studied in the Perth Basin, Western Australia. The aim is to resolve the hydrocarbon saturation and explain the high productivity results, despite the high water saturation, obtained through a conducted formation well test across the interested reservoir zones. A new integration technique between a suite of conventional and advanced logging tools together with the capillary pressure measurements has been carried out to generate a high-resolution reservoir saturation profile, that is lithofacies dependent. Three different independent methods were used in the studied wells to calculate the saturation and to reduce the uncertainty of the final estimated profiles. The methods are the resistivity-based saturation, the NMR-based irreducible saturation, and a new application through saturation height modeling. Furthermore, through the workflow, an effective calibration for the magnetic resonance T2 cutoff has been applied that is supported by the excellent reservoir production behavior from such complex reservoir. The methodology will help resolve the saturation calculation as one of the most challenging reservoir parameters, particularly where the resistivity logs are affected in complicated shaly sand environments. The effectiveness of the workflow shines the possibility to predict high resolution facies and saturation profiles in the lack of resistivity logs. A further possibility can complete the analysis on real time basis, which can certainly provide facies and saturation profiles extended to the uncored wells. Application of this methodology in the uncored wells has shown very encouraging results in various well trajectories, either vertical, deviated or horizontal long boreholes.

1. Introduction

The formation evaluation of complex reservoirs includes several challenges, one of which is the compromised reservoir properties that are dependent on averaged well-logs in shaly sand formations. Accordingly, core analysis played a major role in calibrating the actual rock properties and well logs. Contrary to simple reservoirs, a simple porosity to permeability relationship is no longer valid, so any criteria of log analysis dependent on a supposed simple relation between the rock quality and the reservoir flow are no longer valid. In many reservoir cases, the

* Corresponding author.
E-mail address: a.elkhateeb@postgrad.curtin.edu.au (A. Elkhateeb).
Peer review under responsibility of Southwest Petroleum University.

Production and Hosting by Elsevier on behalf of KeAi

https://doi.org/10.1016/j.petlm.2021.06.004

calculated saturation profile may not represent the hydrocarbon flow proven either by production history, or at least the well testing. In fact, some advanced logs such as the nuclear magnetic resonance (NMR) may provide valuable information, but are considerably different from the actual formation nature, unless they are calibrated to core measurements. In this paper, a comprehensive study in cliff head field is presented through the heterogeneous Early Permian clastic succession in cliff head area. The reservoir sections include the high cliff sandstone formation, defined as interbedded sandstone, conglomerate and siltstone and underlying the Irwin River Coal Measures, Clarke et al. [1]. The formation was deposited in shallow marine to shoreface environments, with the fauna indicating an Artinskian age, Archbold [2]. The overlying Irwin River Coal Measures Formation, introduced by Clarke et al. [1], consists of rapidly alternating siltstone and fined to medium grained sandstone, with carbonaceous shale and lenticular coal beds, McWhae et al. [3] and Mory et al. [4]. The environment of deposition for the Irwin River Coal Measures represents various delta plains, Segroves [5], deposited in the Artinskian age of the Early Permian, McWhae et al. [3]. Further, Mory et al. [6] confirmed the Irwin River Coal Measures as fluvial-deltaic deposits. The top reservoir sand encountered in the Cliff Head area is the Dongara Sandstone of the Kungurian age, Segroves, [5] and Kemp et al. [7]. Mory et al. [6] indicated the age of the Dongara Sandstone was late Early Permian to early Late Permian and described the formation as clean bioturbated silty sandstone underlying the Kockatea Shale, which was equivalent to Beekeeper and Wagina Formations towards the north of the basin. The formation is deposited in shallow marine environment, Rasmussen [8], restricted to the Northern part of the Perth basin, Mory et al. [4]. Fig. 1 shows the stratigraphic column of the Northern Perth Basin and presents the units in the cliff head field, Geoscience Australia [9].

The Irwin River Coal Measures Formation is divided into two very different units, one shaly sand that is the main reservoir in the field, and an underlying tight clean sand. To resolve the saturation profile as one of the most vulnerable rock properties to uncertainty, a new workflow has been applied to 4 wells of variable degree of complexity. The capillary pressure measurements acquired during the special core analyses are utilized to reflect the actual irreducible saturation profile and to calculate the original saturation in thinly bedded zones, McPhee et al. [10]. Moreover, the measurements clearly identify the difference between the different rock types. The shaly sand succession has shown compromised logs resulted in high water saturation at elevated heights in the reservoir. One major challenge in the shaly sands is having productive layers identified as non-reservoir due to the lower facies quality, Bhatti et al. [11]. Rezaee et al. [12] and Al Hinai et al. [13] highlighted the relation between the pore throat size and the permeability in complex rock systems, which reflects a possible high heterogeneity that cannot be resolved through the formation porosity. With the complexity found in the shaly sand rocks, capillary pressure data has been used to resolve for the water saturation profile more accurately. As the reservoir saturation in the log interpretation is dependent on the formation porosity estimated from the conventional logs, an accurate calculation for the reservoir saturation is yet to be challenging through the saturation height modeling workflow. Hence, an independent factor is required to characterize the fluid saturation quantitatively in such complicated reservoir systems.

A new advanced workflow that separates the distribution of the water saturation across the height above the FWL from the formation porosity is presented in this study using 4 wells from cliff head field. The wells have shown an interesting heterogeneity through the clastics succession where the porosity ranges between

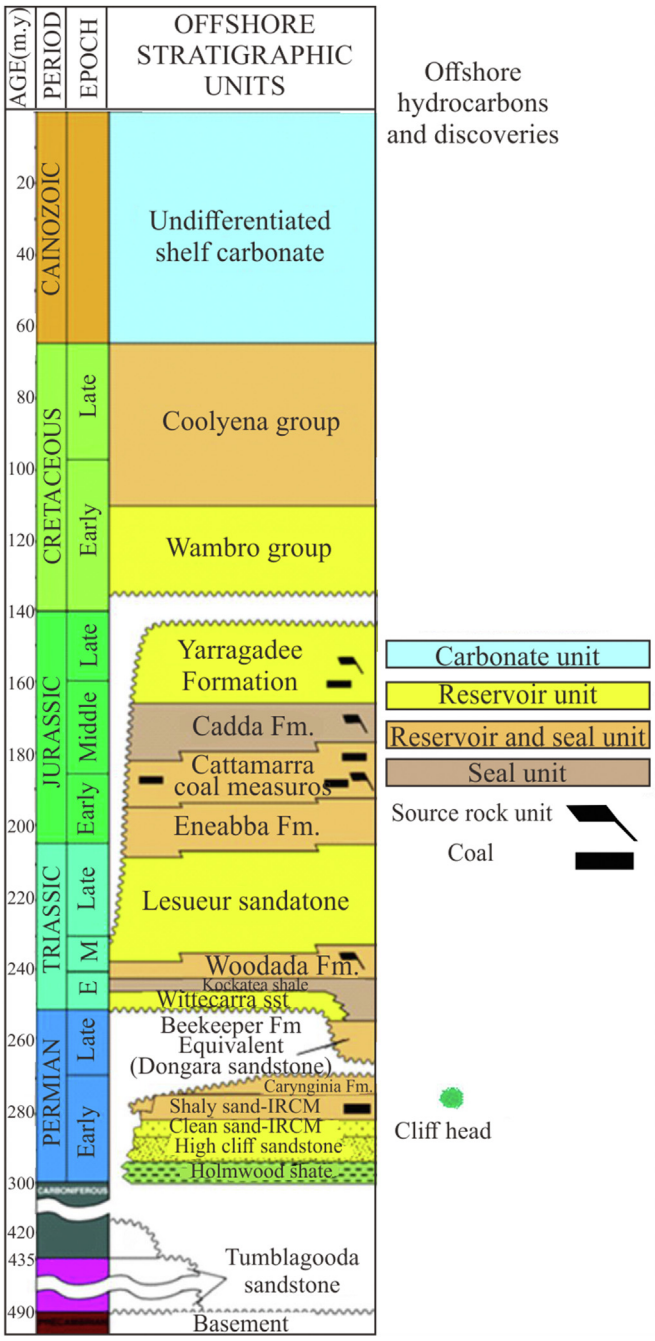

Fig. 1. Stratigraphic column of the Northern Perth Basin in the offshore areas; Modified from Geoscience Australia, 2014.

15% and 25%, while the permeability varies significantly for the same range from tens of millidarcies to nearly 1 Darcy. The EFZI advanced high-resolution electrofacies classification technique is utilized to characterize the electrofacies and the formation permeability, which is verified by core measurements, Elkhateeb et al. [14]. Despite the water saturation was obtained through the resistivity logs, yet the hydrocarbon saturation remains with high uncertainty due to the several factors involved, such as the compromised logs affected by formation shaliness and the reservoir Archie parameters. A more solid evidence of the present uncertainty is that the saturation results through the normal workflow were not reflecting the excellent reservoir production from well testing. To resolve for the accuracy of the formation

saturation profile, an advanced saturation height modeling workflow is generated that is EFZI-dependent. The resulted saturation represented the formation saturation at an irreducible state proven by NMR logs, with the advantage of its applicability in the cored and the uncored wells. The full workflow is described in detail in the following sections.

2. Data and methodology

Four wells were used to test the new saturation height modeling dependent on the equivalent flow zone indicator technique. To build the facies model, routine core measurements through the interested clastics succession were used with a complete set of conventional logs (e.g.: GR, density, neutron, resistivity) in Wells 1 and 3. The NMR is available in Well-1 and 2, with which the water saturation could be calculated independent of resistivity at the irreducible water saturation state. Further, 7 capillary pressure measurements between the two wells are available. A complete advanced petrophysical interpretation was carried out for the four wells, with the log porosity and permeability calibrated to the core routine measurements where applicable. The extended facies in the uncored wells were used to distribute the saturation profile through advanced saturation height modeling. Fig. 2 shows the full workflow adopted in this study for advanced saturation height function modeling.

2.1. Capillary pressure data analysis

The rock capillarity has proven an extraordinary input to the reservoir characterization and saturation evaluation. Two of the three wells in this study were logged by the NMR Tool that covered several zones of interest with considerable reservoir quality differences. Two out of three wells have capillary pressure data, which covered all the target reservoirs. Core porosity and permeability of the studied samples are very variable due to reservoir heterogeneity (Table 1). As can be seen in the Table, there is no good correlation between porosity and permeability due to the reservoir heterogeneity, where the highest porosities show lower permeability relative to the lower porosities.

Fig. 3 shows the capillary pressure measurements done by Centrifuge method for 7 samples classified based on the average permeability values for the plugs, which matches the irreducible water saturation values. The capillary pressure and the measured saturation data were originally measured at lab conditions at very low stresses relative to the reservoir conditions. McPhee et al. [10] confirmed that there is stress relief at atmospheric conditions resulting in an increase in both porosity and permeability of the samples. The application of the Juhaz method yields effective results for stress correction as per the following equations, Juhasz et al. [15].

Table 1
Samples porosity and permeability values.

Sample	Core Porosity (%)	Core Permeability (mD)
S-16	17.4	633.0
S-35	8.8	230.0
S-13	19.7	34.0
S-15	18.5	16.7
S-42	14.8	87.9
S-37	16.5	445.0
S-6	22.1	298.0
S-44	18.1	825.0

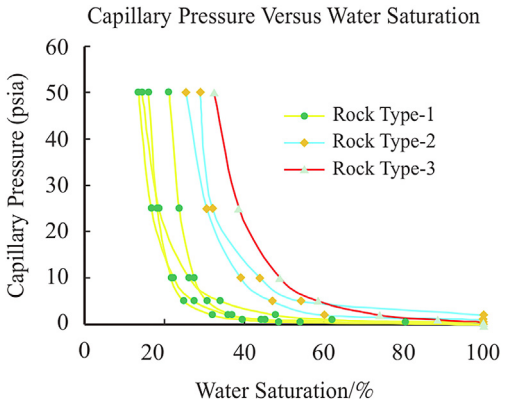

Fig. 3. Capillary pressure data in Cliff Head Field.

$$Pc^* = Pc_{lab}\left[\frac{\varnothing res}{\varnothing lab}\right]^{0.5} \quad (1)$$

$$Sw^*_{nw} = S_{nw_{lab}}\left[\frac{\varnothing res}{\varnothing lab}\right] \quad (2)$$

where Pc^* and Sw^*_{nw} are the stress corrected capillary pressure and plug saturation, Pc_{lab} and $S_{nw_{lab}}$ are the same at ambient conditions.

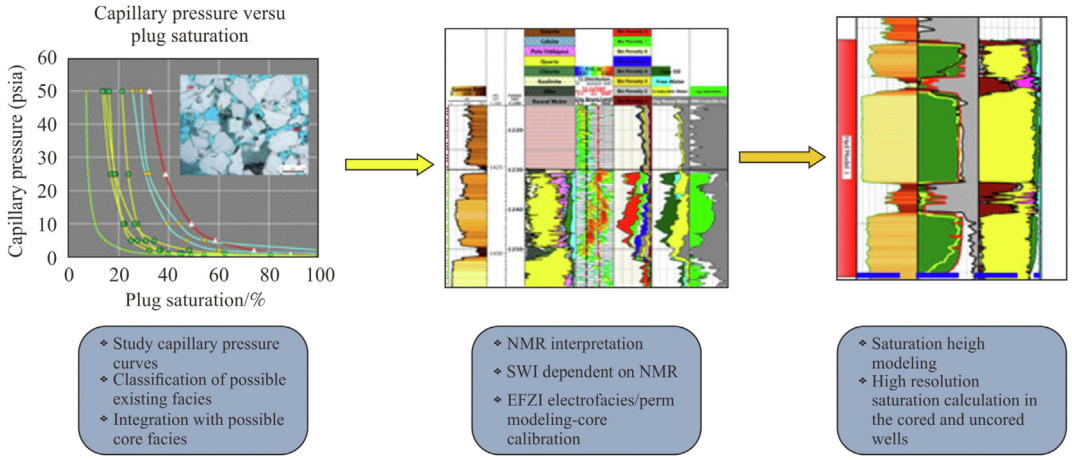

Fig. 2. Workflow used to characterize the reservoir and calculate high resolution rock properties.

The $\varnothing_{lab}$ is the total porosity as measured in the laboratory under the ambient conditions and $\varnothing_{res}$ is the stress corrected porosity. The data requires another correction for reservoir fluids conditions taking into consideration the contact angle and the Interfacial Tension, Purcell [16]. The conversion is done through the following equation:

$$Pc_{res} = Pc_{lab} \times \left[\frac{(\sigma Cos\theta)_{res}}{(\sigma Cos\theta)_{lab}}\right] \quad (3)$$

where the Pc_{res} is the corrected capillary pressure to the reservoir conditions (psia), the θ is the contact angle and the (σ) is the rock interfacial tension (IFT). McPhee et al. [10] have listed the values for the contact angle and the Interfacial Tension in an oil-water system. The contact angle for such system at lab conditions is 0° and the IFT is 72 dyne/cm, while at the reservoir conditions the values are 30° and 30 dyne/cm for the contact angle and IFT respectively. The important application of the capillary pressure concept is how the reservoir fluids are in fact distributed across the thickness of the reservoir prior to its exploitation, Ahmed [17]. A final conversion to reservoir height is required to represent the saturation profile at any certain depth above the reservoir free water level.

$$HAFWL = 144 \times \frac{Pc_{res}}{(\rho_{water} - \rho_{oil})} \quad (4)$$

where HAFWL is the height above the free water level (ft.), ρ_{water} and ρ_{oil} are the densities for the water and oil respectively (lb/ft^3). The saturation height modeling will aim to run a resistivity independent quantitative saturation evaluation and compare it with resistivity-based and the NMR irreducible saturations. Fig. 4 shows the capillary pressure dataset corrected to the reservoir conditions. The left y-axis presents the capillary pressure, while the right side for the same shows the height above the free water level in meters, and the x-axis presents the saturation corrected to reservoir conditions.

2.2. The core thin sections – an integration with the rock capillarity

The target zones in the Irwin river coal measures formation have been covered by core thin sections that allowed further understanding of the reservoir nature. By studying the various thin sections, 4 distinct lithofacies are identified reflecting 4 different rock types, 3 of which are covered by capillary pressure measurements. Fig. 5 shows the first reservoir distinct facies of the poorest quality rock identified in Well-3 at depth 1391.85 m. The rock consists of medium-grained arkose, moderately sorted with potassium feldspars (KF), that is partially replaced by some pyrite locally, and abundant authigenic kaolinite (K.). The permeability of this rock is 4.4 mD, despite that the measured core porosity is 19%. The Kaolinite, identified as dispersed clay by Elkhateeb et al. [14], is clearly filling the pores in the reservoir, which has significantly affected the permeability of this rock type (Rock Type-3). The irreducible water saturation of this facies is 32%.

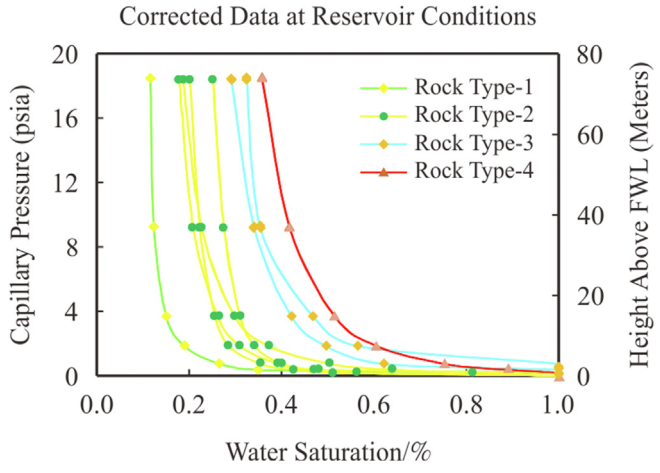

Fig. 4. The corrected capillary pressure measurements to the reservoir conditions.

Rock Type-2 is moderately microporous, medium-grained arkose with abundant authigenic kaolinite that fills the pore spaces. Detrital Clays (Dclay) are presented in this rock type. A clear element that affected the pore volume is the quartz overgrowth (QO). Fig. 6 shows a thin section for Rock Type-2 from Well-2 at depth 1447 m. The porosity and permeability of this sample are 16% and 20.7 mD respectively. In this rock type, the permeability is higher despite the low porosity when compared with RRT-3. The SW_{ir}, based on the PC curves, for this rock type is 27.2%.

The best quality lithofacies in the shaly sand is represented by Reservoir Rock Type-1 in the Irwin River Coal Measures Formation. In this rock type, the pores still have the authigenic kaolin occupying some pores, but with grain to pore structure that reflects much better permeability and clearly identified quartz overgrowth (QO). Fig. 7 shows a thin section that represents this facies with 22% porosity and average permeability value of 550 mD. The irreducible water saturation of this facies is clearly much lower relative to the other two discussed facies with an average value of 16%.

The last identified reservoir rock type (RRT-4) is the low porosity or the tight, clean sand of the Irwin River Coal Measures Formation (Fig. 8). The recorded reservoir properties of this sample is 8.8 porosity units and the permeability is 300 mD, but no valid capillary pressure measurements were recorded for this facies. The clays in this rock are negligible with a clear predominant quartz overgrowth (QO) acting as a cementing agent.

2.3. Identification of reservoir archie parameters

The cored wells have tested the values of the formation resistivity factor and the resistivity index-saturation to estimate the cementation factor (m) and saturation exponent (n) in the different formations. Table 2 summarizes the estimated Archie parameters for each cored formation, Roc Oil, [18].

2.4. Nuclear magnetic resonance

The NMR has been proven a very effective tool that provides a formation porosity independent of reservoir lithology, Coates et al. [19]. A great outcome from the NMR interpretation is the irreducible water saturation (Swi_{NMR}) that can be calculated using the free fluid index (*FFI*) and the NMR porosity (*TCMR*). The following equation was used to calculate the irreducible water saturation:

$$Swi_{NMR} = 1 - \left(\frac{FFI}{TCMR}\right) \quad (5)$$

There are no available core magnetic resonance measurements to identify the precise T2 cutoff. Nevertheless, very solid information about the reservoir productivity had been collected in Well-1 through an extended well test, during which the shaly and the clean sands in well-1 were allowed to flow through 27 m thickness for a continuous 8 days. The reservoir flowed at a rate of 3000 barrels of oil per day with negligible to no water cut, Roc Oil [20]. This will indirectly support a nuclear magnetic resonance interpretation that shows negligible to no free formation water dependent on a selected T2-cutoff value. The final well test results are

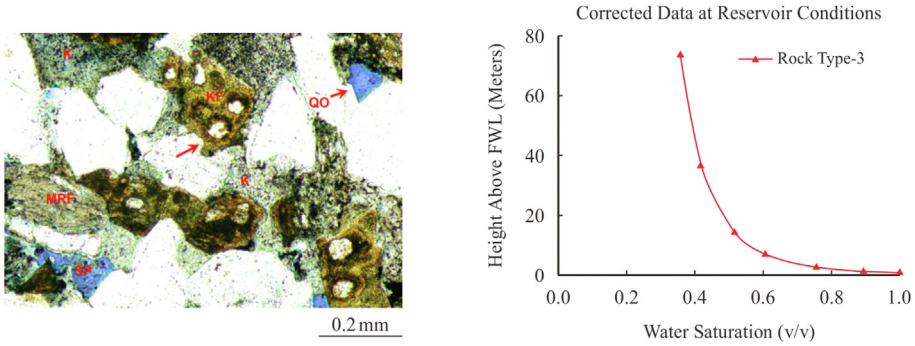

Fig. 5. A core thin section matching the poor quality rock type identified from the capillary pressure curves where the authigenic kaolinite (K) filling the pore spaces, a clear quartz overgrowth (QO) and potassium feldspars (KF) occupied by few pyrite fragments are common in the rock sample.

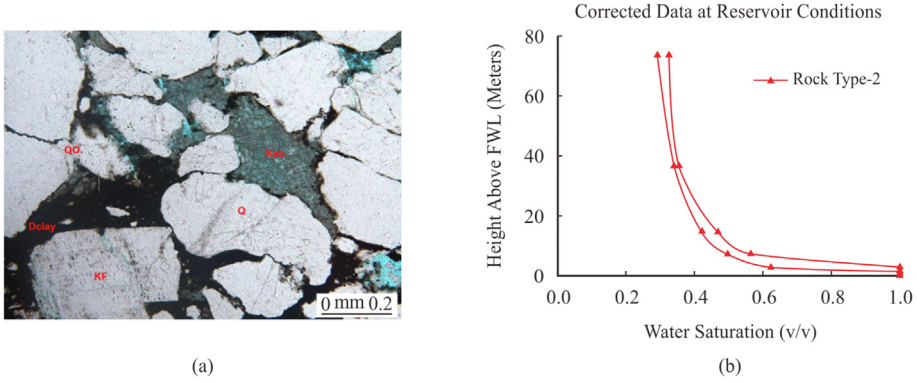

Fig. 6. Thin section for Reservoir Rock Type-2 in which the kaolinite (Kao.) occupies the pore spaces with some detrital clays (Dclay). The quartz overgrowth (QO) is common cementation with the presence of potassium feldspars (KF).

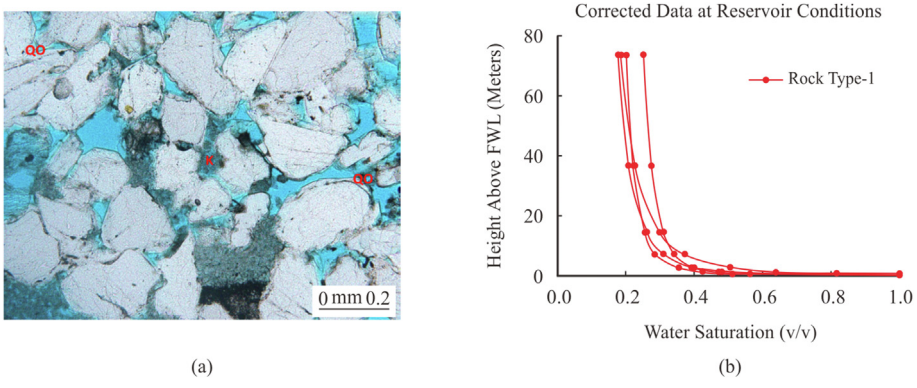

Fig. 7. Thin section showing Reservoir Rock Type-1 reflecting much higher permeability and common intergranular pores relative to other facies. The kaolin (K) still occupies the pore spaces with quartz overgrowth (QO) cementation.

listed in Table 3.

The NMR interpretation has been carried out in wells 1 and 2 to calculate the irreducible saturation and to start the log evaluation for the electrofacies using the equivalent flow zone Indicator (EFZI) method. Several samples from the T2 distribution log have been selected to validate the cutoff, each selected representing a certain rock type from the best quality to the poor quality. The data has been plotted on a semi-log plot versus the T2 relaxation time (Figs. 9 and 10). It is found that all the classified rock types share one valley that separates the small pores with bound fluid from the large pores with free fluids, despite the variance in the logs' signature. A clear variation between the rock types is obvious with a clear variation in the cutoff value, where the shaly sand appears to have a faster cutoff value relative to the clean sands. The shaly sand is found to produce a free fluid volume of net oil at a value of 70 ms, while the clean sands were found to produce the same at a 100 ms T2 cutoff value. Comparing the different rock types classified has revealed also that the volume of the free fluids in the good quality rock (RRT-1) is nearly double the bulk irreducible volume for poor quality rock (RRT-3). Furthermore, upon the application of such variable free fluid cutoff, the NMR interpretation has shown oil-free water matching the well test results. The resulted saturation will

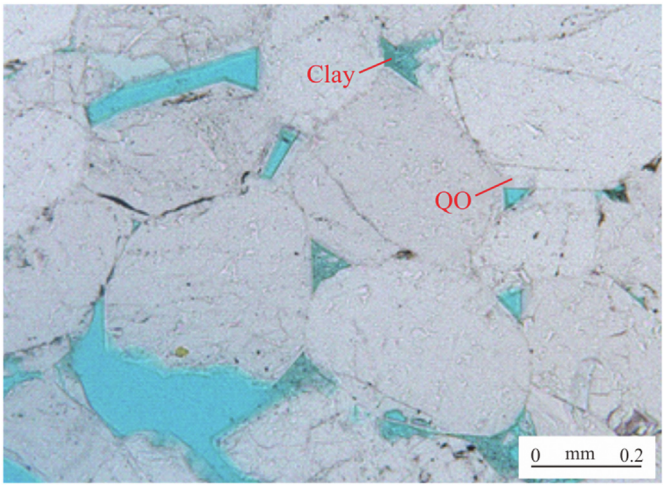

Fig. 8. The Clean Sand facies presenting Reservoir Rock Type-4 in the Irwin River Coal Measures Formation. The rock with intergranular pores that are well interconnected with minor clay content and clear quartz overgrowth (QO) acting as cementing material.

Table 2
Identified Archie parameters in Cliff Head Field for all reservoir rocks.

Formation/Unit	Cementation factor (m)	Saturation exponent (n)
Dongara sandstone	1.98	2.710
Irwin River Coal Measures – shaly sand	1.94	2.754
Irwin River Coal Measures – clean sand	1.91	2.470

represent purely the irreducible water saturation in the reservoir through a resistivity-independent method that has not been affected by any type of mineralogy or formation tightness. The saturation from the NMR interpretation has been compared directly to the resistivity based water saturation calculated using Simandoux shaly sand saturation model, Simandoux [21], which is referred to as the best known of the shaly sand saturation solutions, Cannon [22].

$$\frac{1}{R_T} = \frac{\varnothing^m \times S_w^n}{a \times R_W} + \frac{V_{clay} \times S_w}{R_{clay}} \tag{6}$$

With the availability of complete fluid characterization from the NMR interpretation, the reservoir facies characterization using the Equivalent Flow Zone Indicator technique will be carried out, Elkhateeb et al. [14]. The methodology allows a high-resolution

Table 3
Test results in Well-1 (after Roc Oil, 2003).

Parameters	Well test results
Tested thickness	27 meters
Productivity index	3.00 stb/psi
Permeability-thickness (K-h)	62,500 mD·ft
Pressure depletion	Not indicated
Initial reservoir pressure	1840 psia
Reservoir temperature	75 °C @ 1225 mSS
Water cut	Negligible to none
Oil gravity	31° to 33° API
Viscosity	5.5 to 6.25 cP
GOR	32 to 38 SCF/BBL
Wax	20% with pour point of 33 °C
Asphaltene	<1%

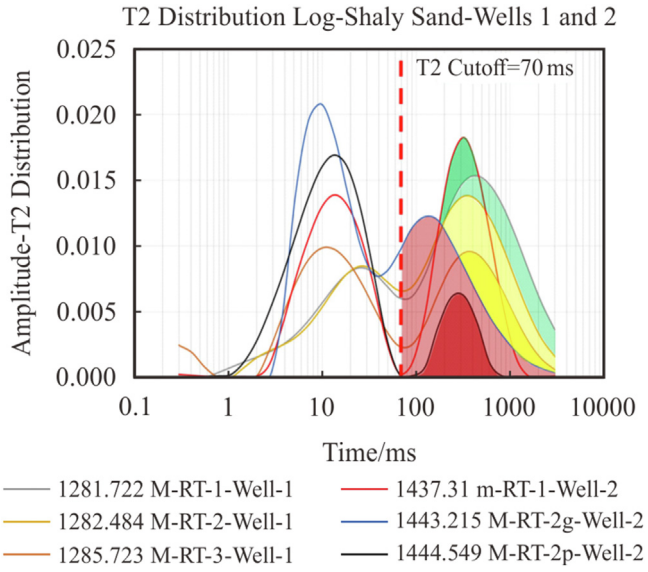

Fig. 9. T2 Distribution log plotted versus relaxation time showing the shared cutoff value for all the shaly sand rock types.

facies log and permeability characterized in heterogeneous reservoirs through the following equation.

$$EFZI = \frac{FFI}{PHID} \tag{7}$$

where the *FFI* is the free fluid index and the *PHID* is the total density porosity.

The classification of the clastics succession in the cliff head field wells started by initializing the EFZI plot on a cumulative frequency chart for all interested zones (Fig. 11). In this plot, several distinct straight lines are formed with each representing a certain hydraulic flow unit, Svirsky et al. [23]. A total of 9 distinct reservoir electrofacies were classified into three formations; 3 for The Dongara Shaly Sands, 4 for The shaly section of the Irwin River Coal Measures and 2 for the underlying tight sands.

Table 4 lists the thresholds of the classification for the 9 identified electrofacies and their relation to the identified reservoir rock types (RRT).

The best application of these identified facies to test them is to run an EFZI-dependent permeability modeling and match the core measurements available in Wells 1 and 3. The hydraulic flow units concept has developed a clustering technique to classify the facies for a reservoir rock, Amaefule et al. [24]. Furthermore, Soleymanzadeh et al. [25] indicated that the flow zone indicator approach is a popular rock type technique that is based on a capillary tube model and hence rock quality index parameter (RQI). Accordingly, in complicated reservoir rocks, a single linear relationship between porosity and permeability cannot describe the rock heterogeneity. Rather the capillarity is reflecting groups of rock types that are connected to a unique permeability model. In general, the different theoretical and empirical correlations between porosity and permeability would require an independent source to calibrate the results, with which simple factors were found to fail to return the proper permeabilities in complex rock textures, Ghadami et al., [26]. The FZI is considered an independent factor that showed consistency in the nature of the various rock types, Elkhateeb et al., [27] and Garrouch et al., [28]. To calculate the flow zone indicator, the rock quality index (RQI) is calculated using the following equation:

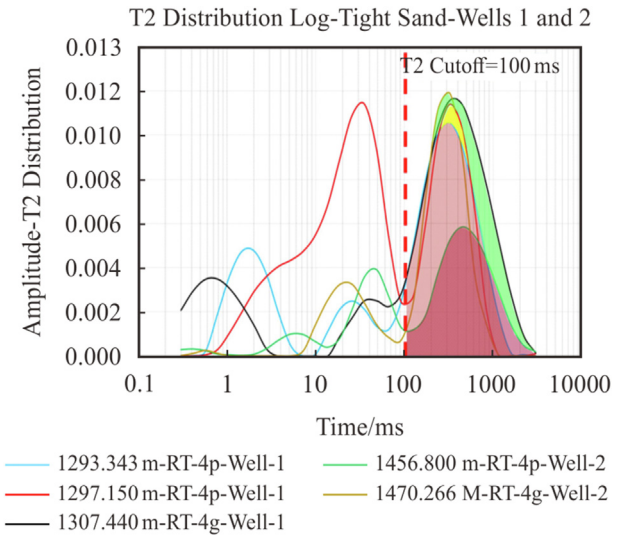

Fig. 10. T2 Distribution log plotted versus relaxation time showing the shared cutoff value for all NMR log samples from the clean tight sand rock type.

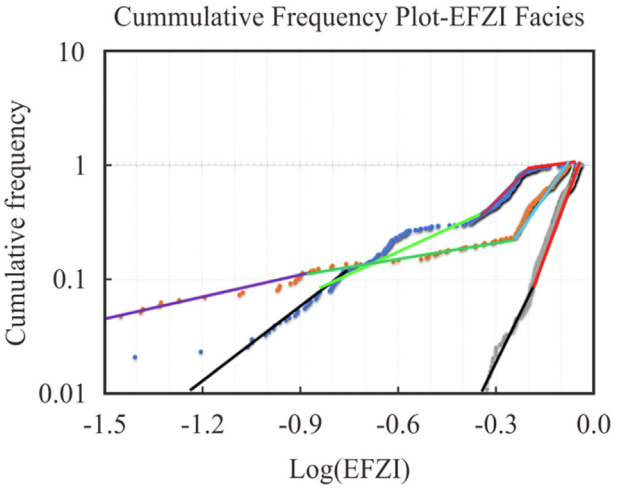

Fig. 11. Cumulative frequency chart for the available facies in the Cliff Head Field Clastics succession.

$$RQI = 0.0314 \times \sqrt{\left(\frac{k}{\phi}\right)} \tag{8}$$

where the ϕ is the core plug porosity, and k is the plug permeability. A normalization (ϕ_z) for the measured core porosities (ϕ) has been carried out through the following equation:

$$\phi_z = \frac{\phi}{1-\phi} \tag{9}$$

The final FZI is defined as:

$$FZI = \frac{RQI}{\phi_z} = \frac{0.0314 \times \sqrt{k/\phi}}{\frac{\phi}{1-\phi}} \tag{10}$$

2.5. The high-resolution saturation height modeling

The saturation height modeling has been carried out to characterize the saturation in the clastics succession in Cliff Head Field. In order to set up the variation between the previously defined rock typing models, an integration between the classified EFZI facies and the capillary pressure saturation height has been done to model an effective high-resolution saturation profile. Using the Leverett-J Function modeling for each rock type, a saturation height function has been defined to fit each of the classified rock types independently as per the following models. Fig. 12 shows the J-Function versus water saturation for each rock type.

$$Swi_{RRT-1,4} = 0.05875/(J + 0.03629) + 0.22766 \tag{11}$$

$$Swi_{RRT-2} = 0.03867/(J - 0.01391) + 0.31961 \tag{12}$$

$$Swi_{RRT-3} = 0.36872 \times J^{-0.257} + 0.0487 \tag{13}$$

where (J) is the Leverett-J Function, Ahmed [17], calculated as per the following equation:

$$J = 0.21645 \times \left(\frac{Pc}{\sigma Cos\theta}\right) \times \sqrt{\frac{K}{\varnothing}} \tag{14}$$

where Pc is the capillary pressure, K is the EFZI-dependent formation permeability, and ∅ is the calculated formation porosity. The saturation height modeling has been carried out using the rock typing classified for the clastics succession, further extended to the uncored horizontal well, which had a considerable offset to the free water level, through a long high heterogenous drilled section.

The saturation height modeling will act as a third independent water saturation computation across the target zones for all rock types. In such a complicated reservoir, it is very hard to allocate the correct saturation-height model to a certain rock type where the porosity is not a discriminating factor. Yet, the permeability solely

Table 4
The identified Rock Types and the electrofacies classification using the Equivalent Flow Zone Indicator technique.

Formation	Reservoir rock type (RRT)	Hydraulic flow unit *(HFU)*	Cumulative frequency threshold *log (EFZ)*
Dongara sandstone	RRT-3	HFU-1	<-0.87
	RRT-2	HFU-2	>-0.87, >-0.24
	RRT-1	HFU-3	>-0.24
Irwin River Coal Measures – Shaly sand and high cliff sandstone	RRT-3	HFU-4	<-0.8
	RRT-2	HFU-5	>-0.8, < −0.34
		HFU-6	<-0.18
	RRT-1	HFU-7	>-0.18
Irwin River Coal Measures – Clean sand	RRT-4	HFU-8	<-0.17
		HFU-9	>-0.17

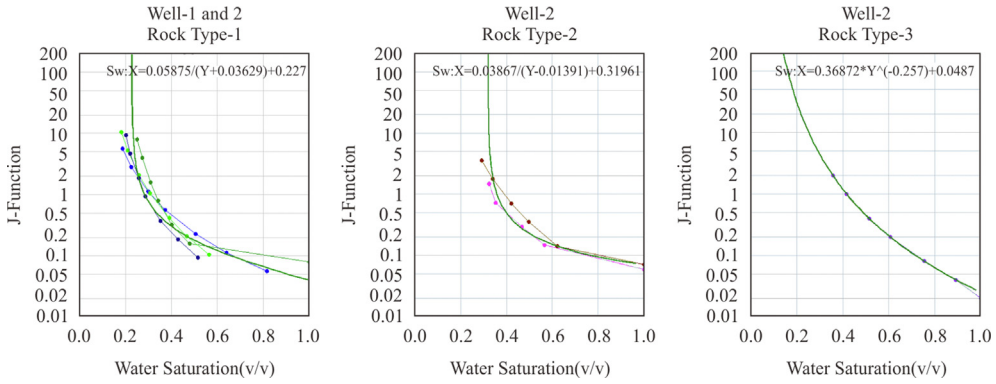

Fig. 12. Leverett-J plotted against the water saturation for the capillary pressure corrected curves.

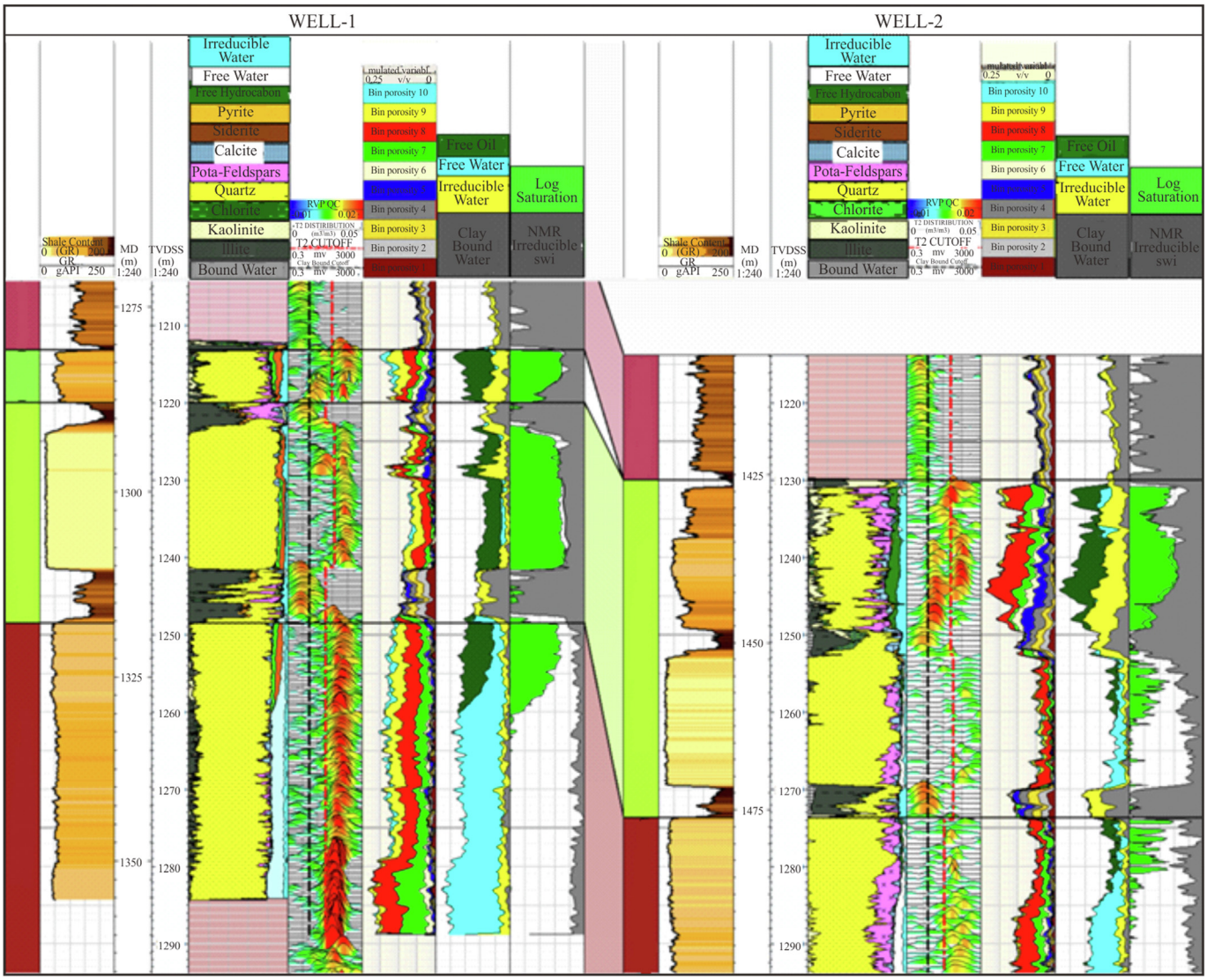

Fig. 13. Petrophysical analysis and NMR interpretation integration in Wells 1 and 2. Track-1: GR log, scaled from 0 to 250 GAPI, with shading indicating the formation shaliness; Track-2: The mineralogical petrophysical modeling, scaled from 0 to 1, showing the shale comprises of three clay types, kaolinite, Illite and chlorite; Track-3: The NMR T2-Distribution array with two cutoffs, the clay bound water (black) and the variable T2 cutoff (red) all scaled from 0.3 to 3000 ms; Track-4: The NMR bin porosities based on the different time partitions scaled from 0 to 25 porosity units; Track-5: The NMR interpretation showing the clay bound water (grey), the irreducible water (yellow), the free water (cyan) and the free hydrocarbons (dark green), all scaled from 0 to 25 porosity units; Track-6: The calculated water saturation logs from the resistivity (green shaded) and the NMR interpretation reflecting the irreducible water saturation (reverse shading in grey), all scaled between (1–0).

cannot act as a final defining factor since there could be two facies of high and low permeabilities that are showing the same porosity. To assign the correct saturation model to a certain rock type, at a specific reservoir height, the EFZI facies and the permeability were integrated in the saturation height modeling workflow based on the following equation:

$$S_{wi} = f(K_i\ ,\ EFZI_i) \tag{15}$$

In cliff head field, the resulted saturation profile will represent the reservoir at its irreducible state due to the oil-free water produced in the well testing. Furthermore, the modeling can be used on a real time basis, with the lack of resistivity logs, where the water saturation can be calculated while drilling through the characterized facies log using equations (11)–(13).

3. Modeling results

This integrated formation evaluation has allowed the development of a new workflow to characterize two formation properties quantitatively, permeability, and water saturation. Moreover, a generation of the irreducible water saturation as a continuous log has the possibility to extend the results to any uncored well. Further, an independent calibration was given for the T2 cutoff value for the magnetic resonance log interpretation.

3.1. Petrophysical evaluation and NMR interpretation results

The petrophysical interpretation has been carried out, applying the SCAL determined Archie parameters, using the mineralogical inversion analysis. The clays used in the evaluation are the kaolinite and illite as the main clays in the zones of interest proven by the core examination. Wells 1 and 2 NMR logs were interpreted to provide an independent source for the saturation calculation, which will be compared relative to the calculated saturation based on resistivity and porosity logs. Fig. 13 shows a correlation between wells 1 and 2. Track-1 shows the Gamma ray log; Track-2 shows the mineralogical petrophysical interpretation for both wells integrated with the analyzed fluid characterization from the NMR interpretation; Track-3 shows the T2 distribution log with the variable T2 cutoffs; Track-4 presents the porosity bins partitioned to 10 partial porosities (1, 2, 4, 8, 16, 33, 100, 300, 1000 and 3000 ms). Clearly, there is a difference in the pore structure where the bin porosity 9 constitutes the majority of the pores in Dongara Shaly sands relative to bin porosity 8 in the Irwin River Coal Measures Shaly Sand, which indicates a smaller pore size for the latest proven by the core thin sections. Track-5 presents the NMR interpretation utilizing the variable T2 cutoffs where the grey is the clay bound water, the yellow is the small pore bound water porosity, and the free fluids are partitioned into two volumes: Free water in blue and the free hydrocarbons in dark green. Track-6 presents the calculated irreducible water saturation from the NMR interpretation shaded in grey, while the resistivity log-based Simandoux water saturation is shaded in green.

There is a very good match between the two saturations in the shaly sand intervals (Dongara and Irwin River Coal Measures) despite the very different sources of the calculated saturations. There is a clear variance between the two logs in Well-1 in the High cliff sandstone formation and in the tight sand in Well-2, above the

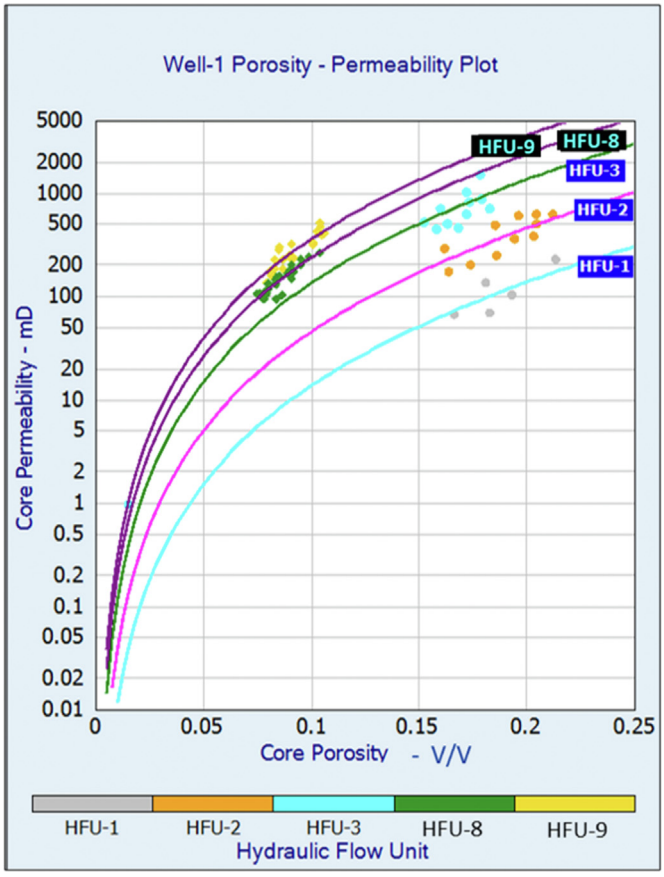

Fig. 14. Porosity vs. Permeability plot showing the HFUs classification in the Dongara and the clean sands of the Irwin River Coal Measures Formation.

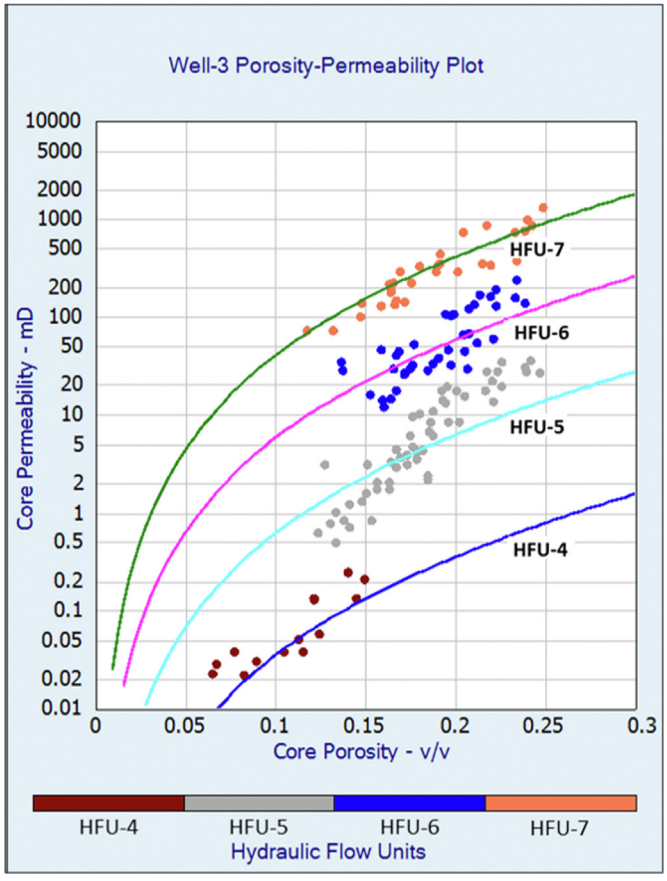

Fig. 15. Porosity vs. Permeability plot showing the HFUs classification in the shaly sands of the Irwin River Coal Measures Formation.

contact at 1261 mSS. One would interpret this as a transition zone in which it is possible to have an increased free water volume next to the reservoir hydrocarbon fluids. However, the facies in the High cliff sandstone formation are represented by the best quality rock type, with which it is expected to have a thinner transition zone. The saturation height modeling will confirm the actual saturation in this zone.

3.2. Permeability calculation

The permeability has been calculated utilizing the core-based classified electrofacies equations through the porosity-permeability plot in Well-1 and Well-3. The two wells are for different formations of different reservoir characteristics, therefore they have been separated into two different plots, one for the Dongara Sandstone and the Irwin River Coal Measures clean sands in Well-1, and the second for Shaly sands of the Irwin River Coal Measures in Well-3 as shown in Fig. 14 and Fig. 15 respectively.

Nine permeability models have been used to run the permeability calculations for all the facies. For the Dongara sandstone and the tight clean sands, the equations are:

$$K_{HFU1} = \varnothing^3 \times (3.305/(0.0314 \times (1 - Phi))^2 \quad (16)$$

$$K_{HFU2} = \varnothing^3 \times (6.03/(0.0314 \times (1 - Phi))^2 \quad (17)$$

$$K_{HFU3} = \varnothing^3 \times (10.376/(0.0314 \times (1 - Phi))^2 \quad (18)$$

$$K_{HFU8} = \varnothing^3 \times (13.796/(0.0314 \times (1 - Phi))^2 \quad (19)$$

$$K_{HFU9} = \varnothing^3 \times (16.933/(0.0314 \times (1 - Phi))^2 \quad (20)$$

For the shaly sands of the Irwin River Coal Measures, the following equations have been utilized, Elkhateeb et al. [14]:

$$K_{HFU4} = Phi^3 \times (0.203/(0.0314 \times (1 - Phi))^2 \quad (21)$$

$$K_{HFU5} = Phi^3 \times (0.761/(0.0314 \times (1 - Phi))^2 \quad (22)$$

$$K_{HFU6} = Phi^3 \times (2.248/(0.0314 \times (1 - Phi))^2 \quad (23)$$

$$K_{HFU7} = Phi^3 \times (5.5/(0.0314 \times (1 - Phi))^2 \quad (24)$$

From the cross plots, it is clear the significant variance between the rock types, particularly in the shaly sands. There is an overlap for the reservoir porosity with variance in the permeability of several orders of magnitudes. Fig. 16 presents the results of the high-resolution EFZI facies and the permeability logs.

The wells are showing the gamma ray log in Track-1; Track-2 shows the porosity logs, density in red and neutron in blue; Track-3

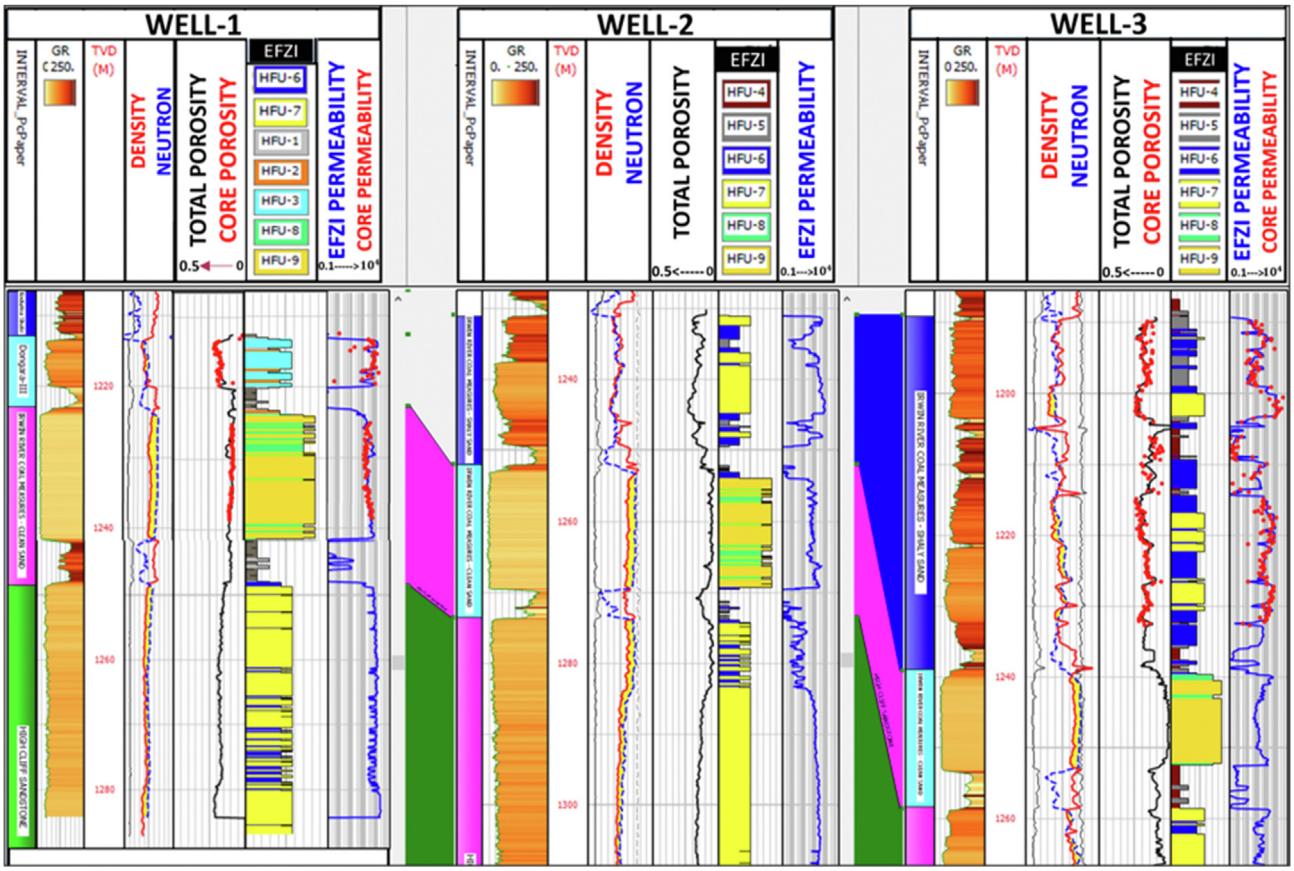

Fig. 16. The EFZI classified facies and the calculated permeability showing a very good match to the core permeability. Track-1: The GR log, scaled from 0 to 250 GAPI, with the shading indicating shaliness of the formation; Track-2: The density (red) scaled from (1.95–2.95 g/cc) and the neutron (blue) scaled from (0.45 – (–0.15)) according to the limestone scale; Track-3: The calculated total porosity (black) and where applicable, in wells 1 and 3, the core plug porosity (red dots) plotted showing a very good match to log porosity; Track-4: The classified equivalent flow zone indicator facies (EFZI); Track-5: The EFZI permeability (blue) showing a good match with the core permeability (red) in wells 1 and 3, both scaled between 0.1 and 10,000 mD.

shows the core porosity in Wells 1 and 3 matching very well the log calculated porosity in Black; Track-4 shows the EFZI facies; Track-5 presents the EFZI high resolution permeability log matching the core permeability in wells 1 and 3. From the results, the porosity in the shaly sands in Wells-2 and 3 seem to be consistent in the range, however, the permeability varies, as the facies identified, significantly between the sand layers. This is where the capillarity effect reflects the interaction between the rock and fluids, controlled by pore geometry in such case, Harrison and Jing [29].

3.3. Saturation height modeling

The saturation height modeling is considered another independent evaluation for the saturation profile from a completely independent source. In cliff head field, the water saturation profile is representing the irreducible water saturation for all the reservoir intervals proven by well testing. Studying the capillarity behavior of the various rock types revealed a connection to the permeability of the rock rather than the porosity. The EFZI methodology results have provided a quantitative facies heterogeneity model, with which the calculated permeability has shown a great match with the core permeability. In the saturation height modeling process, two independent factors have been integrated to calculate a high-resolution water saturation profile above the free water level, which are the EFZI classified facies and the high-resolution permeability. The capillary pressure curves at reservoir conditions have been converted to the height above the free water level using equation (4). Following the conversion, the application of equations (11)–(14) yields an independent saturation profile in both the cored and the uncored wells.

Several combined thresholds between the permeability and the EFZI facies have been utilized to distribute the reservoir fluids into the rock at the different heights above the reservoir contact.

$$Swi_{RRT-1,} = f(K(>150 \leq 1000\ mD),\ HFU-3\&7,\ 8\&9) \tag{25}$$

$$Swi_{RRT-2} = f(K(>20 \leq 150\ mD),\ HFU-2,5\&6) \tag{26}$$

$$Swi_{RRT-3} = f(K \leq 20\ mD,\ HFU-1\&4) \tag{27}$$

Fig. 17 presents the results of the high-resolution saturation height modeling in the first 3 wells. The reservoir extends up to

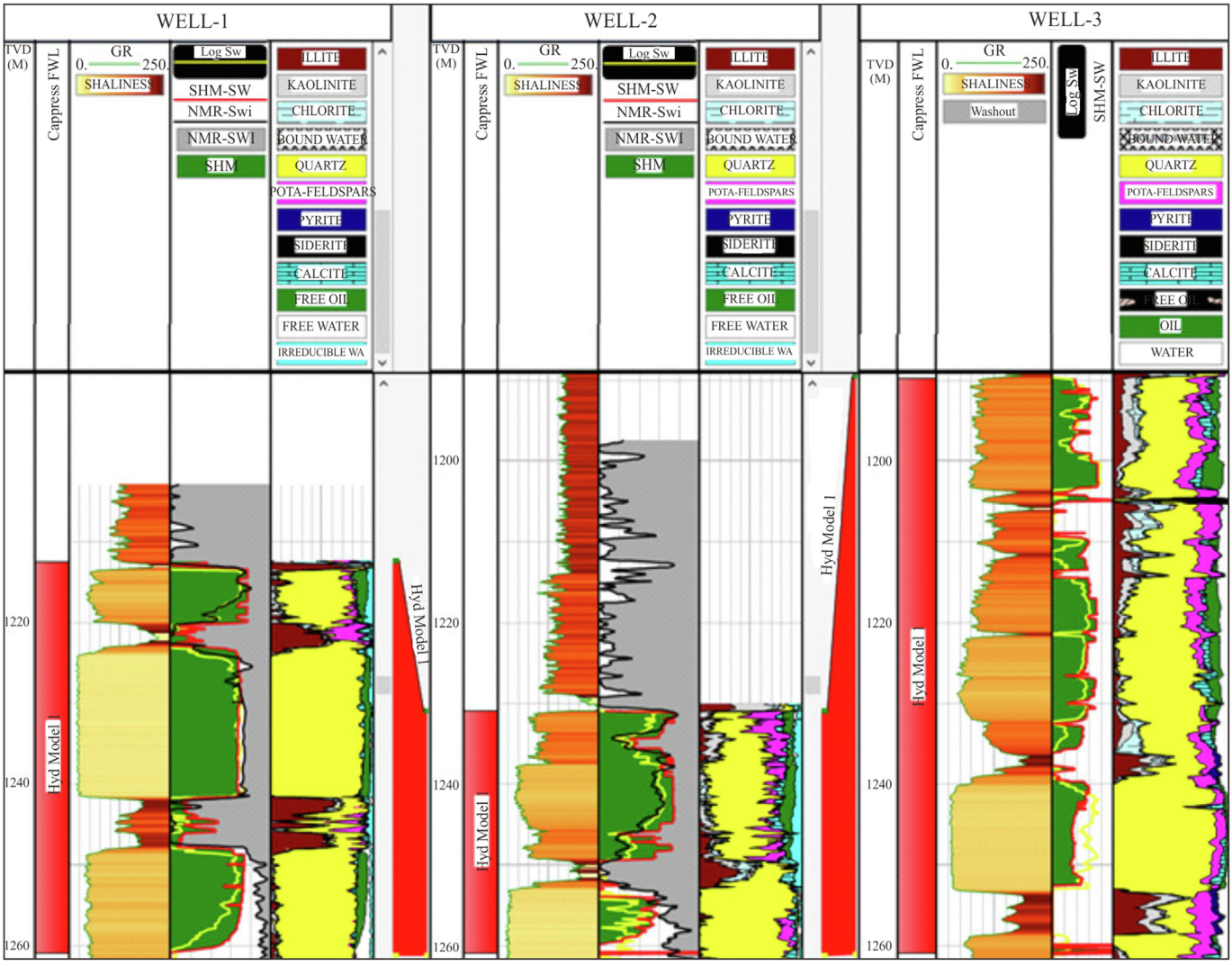

Fig. 17. Saturation Height Modeling results based on the EFZI facies modeling. Track-1: The GR log scaled from 0 to 250 GAPI; Track-2: The calculated water saturation from the different applications, scaled from (1–0), first the resistivity based model (yellow), second the irreducible water saturation from NMR (black) and the saturation height modeling (red); Track-3: The mineralogical petrophysical modeling scaled from 0 to 1.

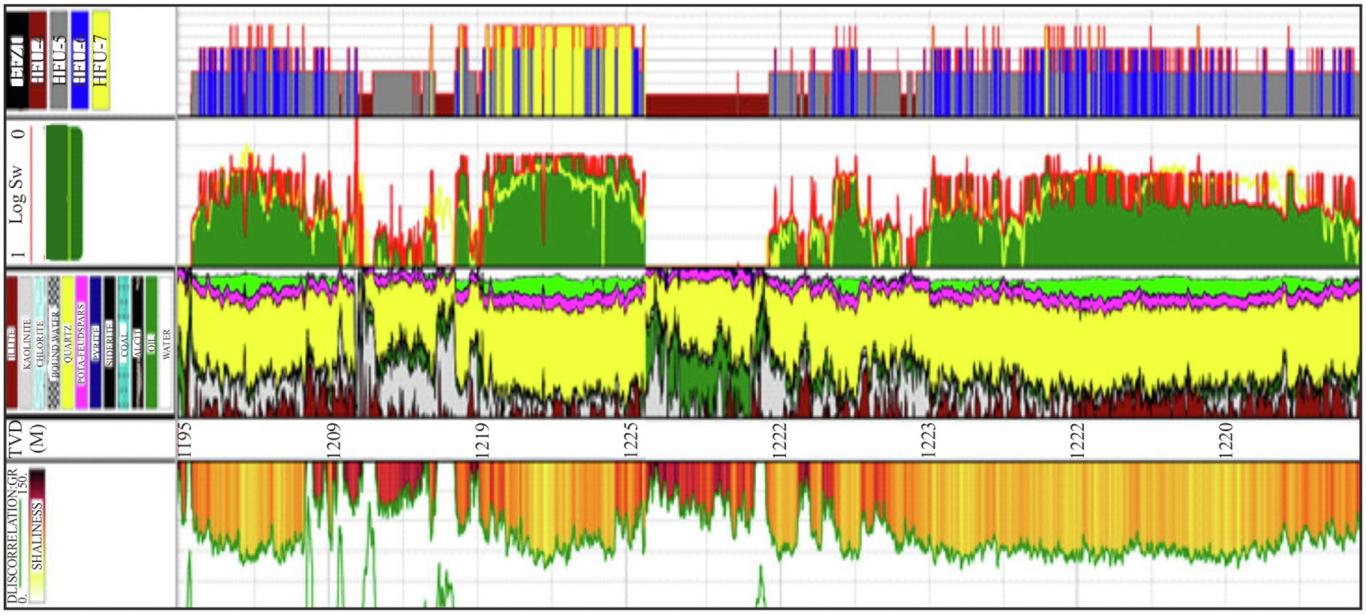

Fig. 18. Well-4 testing the EFZI-Based saturation height modeling through a long horizontal well with a high degree of facies variation. Track-1: The GR log scaled between 0 and 150 GAPI with shading indicating shaliness of the formation; Track-2: The mineralogical petrophysical modeling; Track-3: The calculated water saturation from the different applications scaled from (1–0), the resistivity based model (yellow) and the saturation height modeling (red); Track-4: The EFZI classified facies.

71 m true vertical thickness above the free water level in Well-3, which will help to test the integration methodology on a long vertical thickness of the reservoir. Track-1 shows the Gamma ray log; Track-2 shows the different water saturation logs calculated using 3 different methods. The yellow is the resistivity based SW; the red is the saturation height modeling (SHM-SW) dependent on the EFZI facies; and the black is the SWI from NMR interpretation.

The results have shown very interesting coherency where the log-based water saturation (Yellow) has matched the NMR irreducible saturation (Black) and the saturation height modeling (Red) in Well-1. This indicates valid Archie parameters and proves the validity of the variable NMR T2 cutoff applied in the interpretation, calibrated to measured Archie parameters from the SCAL measurements. The saturation height modeling has shown extraordinary results upon a calibrated core facies and calibrated permeability log. In the sandstone section above the FWL in Wells 1 and 2, the new saturation height model results showed the true saturation for such facies with thin transition zone matching the best quality rock type, which was not accurately addressed in the resistivity based saturation. The shaded red zones next to the depth track are representing the height above the free water level (1261 mSS) where Well-3 has encountered the thickest hydrocarbon thickness among the three wells. In Wells 2 and 3, the results have shown some variance relative to the log-based Simandoux saturation due to that the resistivity is suppressed by the formation shaliness, which resulted in averaging the resistivity value for the sands and shales. On the other hand, the Lower section in Well-3 below 1240 mSS in the clean tight reservoir of the Irwin River Coal Measures Formation shows the log-based SW lower than the modeled saturation. This is due to the formation tightness that affects the resistivity log values. Accordingly, the application of this workflow allows the calculation of the water saturation in the absence of any resistivity log in the borehole.

The modeling workflow has been extended further and tested on the fourth well that was drilled horizontally through the shaly sand of the Irwin River Coal Measures Formation (Fig. 18). The long section was drilled with an offset of 45 m above the FWL, at the highest point of the structure, and encountered a complex facies variation along the lateral section. The reservoir shows high heterogeneity with high shale content and intercalation between shales and sands, which resistivity response will not account for. The modeled saturation profile has shown much higher resolution saturation profile that is originally based on the core data and extended to the subject well.

It is believed that the methodology can be used as a high-resolution real time workflow to provide three petrophysical parameters of high challenge, the facies, the permeability, and the saturation profile all on high resolution mode.

4. Conclusions

An integrated workflow has been carried out to validate and reduce the uncertainty in the water saturation through the high heterogeneous formations. Four wells have been used to test the workflow that were drilled through the Early Permian clastics succession in the Perth Basin. The core capillary pressure data was found to describe 4 different reservoir lithofacies supported by core thin sections in 3 different formations. In the light of the identified lithofacies, the EFZI methodology was utilized to classify nine electrofacies across all the interested reservoir sands upon which the permeability log has been calculated. A very good match to the core permeability has been achieved. The water saturation involved a challenge to accurately estimate for each reservoir facies due to the high irreducible saturation found in the shaly sands. Therefore, three methods were used to calculate the saturation profile: A resistivity-based water saturation, the NMR irreducible water saturation utilizing variable T2 cutoffs and an EFZI dependent saturation height modeling. The results were found to be very encouraging and supported by an extended Drill Stem Test during which negligible oil-free water was produced for a long period of time. The integrated workflow was tested in four wells of different degree of complexity, which showed very consistent results. The EFZI dependent saturation height modeling is a proven very effective tool to estimate the water saturation in high

heterogeneous rocks, which can be extended to any uncored wells. The workflow can be used as a real time estimation for the permeability and saturation profiles in deviated and horizontal wells in the absence of formation resistivity log.

Acknowledgements

The authors of this paper would like to acknowledge the contribution of The Government of Western Australia [30] for supporting this research, and for making the data used in this study available in an easy comprehensive fashion. With great appreciation, the authors acknowledge the contribution of Schlumberger and Lloyd's Register Digital Products Limited for providing the software used in the evaluation.

References

[1] E. Clarke, C. de, K.L. Prendergast, C. Teichert, R.W. Fairbridge, Permian succession and structure in the Northern part of the Irwin River area, Western Australia, J. Roy. Soc. West Aust. 35 (1951) 31–84, 1951, https://www.biodiversitylibrary.org/part/299451.
[2] N.W. Archbold, Studies on Western Australian Permian Brachiopods 14. The fauna of the Artinskian high Cliff sandstone, Perth basin, Proc. Roy. Soc. Vic. 109 (1997) 199–231.
[3] J.R.H. Mcwhae, P.E. Playford, A.W. Linder, B.F. Glenister, B.E. Balme, The stratigraphy of Western Australia, J. Geol. Soc. Aust. 4 (2) (1958) 1–161, https://doi.org/10.1080/00167615608728471.
[4] A.J. Mory, D.W. Haig, S. Mcloughlin, R.M. Hocking, Geology of the Northern Perth Basin, Western Australia, a Field Guide: Western Australia Geological Survey, Record 2005/9, 2005, pp. 35–39.
[5] K.L. Segroves, The sequence of palynological assemblages in the Permian of the Perth basin, Western Australia, in: Proceedings and Papers of the Second International Gondwana Symposium, Johannesburg, South Africa, 1970, 1971, pp. 511–529.
[6] A.J. Mory, R.P. Iasky, Stratigraphy and Structure of the Onshore Northern Perth Basin, Western Australia, vol. 46, Western Australia Geological Survey, Report, 1996, pp. 13–17.
[7] E.M. Kemp, B.E. Balme, R.J. Helby, R.A. Kyle, G. Playford, P.L. Price, Carboniferous and Permian palynostratigraphy in Australia and Antarctica — a review, BMR (Bur. Miner. Resour.) J. Aust. Geol. Geophys. 2 (1977) 177–208, 1977.
[8] B. Rasmussen, Petrology and Stratigraphy of Subsurface Sandstones Near the Permo-Triassic Boundary, Northern Perth Basin, Western Australia [thesis], University of Western Australia, 1986, p. 126.
[9] Geoscience Australia, Perth basin, province and sedimentary basin geology, Northern Perth basin stratigraphy. http://www.ga.gov.au/scientific-topics/energy/province-sedimentary-basin-geology/petroleum/offshore-southwest-australia/perth-basin#heading-2, 2014 accessed 11 November 2020.
[10] C. McPhee, J. Reed, I. Zubizarreta, Preparation for special core analysis, chapter 6 and 9, in: J. Cubitt (Ed.), Core Analysis: A Best Practice Guide, Development in Petroleum Science Series, Holt, Wales, 2015, pp. 297–298, 508-511.
[11] A.A. Bhatti, A. Ismail, A. Raza, R. Gholami, R. Rezaee, R. Nagarajan, E. Saffou, Permeability prediction using hydraulic flow units and electrofacies analysis, J. Energy Geosci. 1 (2020) 81–91, https://doi.org/10.1016/j.engeos.2020.04.003, 2020.
[12] M.R. Rezaee, A. Jafari, E. Kazemzadeh, Relationships between permeability, porosity and pore throat size in carbonate rocks using regression analysis and neural networks, J. Geophys. Eng. 3 (2006) 370–376, https://doi.org/10.1088/1742-2132/3/4/008, 2006.
[13] A. Al Hinai, R. Rezaee, A. Saeedi, R. Lenormand, Permeability prediction from mercury injection capillary pressure: an example from the Perth basin, Western Australia, APPEA J. 53 (2013) 31–36, 2013, http://hdl.handle.net/20.500.11937/30149.
[14] A. Elkhateeb, R. Rezaee, A. Kadkhodaie, Prediction of high-resolution facies and permeability, an integrated approach in the Irwin River coal Measures Formation, Perth basin, Western Australia, J. Petrol. Sci. Eng. 181 (2019) 1–12, https://doi.org/10.1016/j.petrol.2019.106226, 2019.
[15] I. Juhasz, The Central Role of Qv and Formation-Water Salinity in the Evaluation of Shaly Formations, Society of Petrophysicists and Well-Log Analysts, 1979.
[16] W.P. Purcell, Capillary Pressures – Their Measurement Using Mercury and the Calculation of Permeability Therefrom, Society of Petroleum Engineers, 1949. https://doi:10.2118/949039-G.
[17] T. Ahmed, Fundamental of Rock Properties, Chapter 4, Reservoir Engineering Handbook, second ed., Gulf Professional Publishing Company, Houston, Texas, 2001, pp. 183–278, 2001.
[18] Roc Oil Company, A Special Core Analyses Study of Selected Samples, A Core Lab Report, 2004. April 2004.
[19] R.G. Coates, L. Ziao, M.G. Prammer, NMR Logging Principles and Applications, Halliburton Energy Services Publication H02308, Houston, USA, 1999.
[20] Roc Oil Company, 2003, Cliff Head-3 Corehole-1 Well Completion Report, Part-2 Interpretation, December 2003.
[21] P. Simandoux, Dielectric measurements on porous media application to the measurement of water saturations: study of the behaviour of argillaceous formations, Rev. Inst. Fr. Petrol 18 (Suppl) (1963) 193–215.
[22] S. Cannon, Evaluation of lithology, porosity and water saturation,, in: Petrophysics: A Practical Guide, Chapter-6, John Wiley & Sons, Incorporated, 2015. ProQuest eBook Central, 2016. https://ebookcentral.proquest.com/lib/curtin/detail.action?docID=4038302.
[23] D. Svirsky, A. Ryazanov, M. Pankov, P.W.M. Corbett, A. Posysoev, Hydraulic flow units resolve reservoir description challenges in a siberian oil field, in: Paper SPE-87056, Presented at the SPE Asia Pacific Conference on Integrated Modelling for Asset Management, Kuala Lumpur, Malaysia, 29-30 March, 2004.
[24] J.O. Amaefule, M. Altunbay, D. Tiab, D.G. Kersy, D.K. Keelan, Enhanced reservoir description: using core and log data to identify hydraulic (flow) units and predict permeability in uncored intervals/wells, in: Paper SPE-26436, Presented at 68th Annual Technical Conference and Exhibition of the Society of Petroleum Engineers, 1993, pp. 3–6. Houston, Texas.
[25] A. Soleymanzadeh, M. Jamialahmadi, A. Helalizadeh, B.S. Soulgani, A new technique for electrical rock typing and estimation of cementation factor in carbonate rocks, J. Petrol. Sci. Eng. 166 (2018) 381–388, https://doi.org/10.1016/j.petrol.2018.03.045, 2018.
[26] N. Ghadami, M.R. Rasaei, S. Hejri, A. Sajedian, K. Afsari, Consistent porosity-permeability modeling, reservoir rock typing and hydraulic flow unitization in a giant carbonate reservoir, J. Petrol. Sci. Eng. 131 (2015) 8–69, https://doi.org/10.1016/j.petrol.2015.04.017, 2015.
[27] A. Elkhateeb, R. Rezaee, A. Kadkhodaie, Log dependent approach to predict reservoir facies and permeability in a complicated shaly sand reservoir, ASEG Ext. Abstr. 1 (2019) 1–5, https://doi.org/10.1080/22020586.2019.12072924, 2019.
[28] A.A. Garrouch, A.A. Al-Sultan, Exploring the link between the flow zone indicator and key open-hole log measurements: an application of dimensional analysis, J. Petrol. Geosci. 25 (2018) 219–234, https://doi.org/10.1144/petgeo2018-035, 2019.
[29] B. Harrison, X.D. Jing, Saturation height methods and their impact on volumetric hydrocarbons in place estimates, in: Presented at SPE Annual Technical Conference and Exhibition Held in New Orleans, 2001. Louisiana, USA, September 30 – October 3rd.
[30] Government of Western Australia, Department of Mines, industry regulation and safety, Australia, public domain of Western Australian data website (WAPIMS), data retrieved from, https://wapims.dmp.wa.gov.au/WAPIMS/Search/Wells. accessed 20 December 2018.

Nomenclature

BVW: Bulk volume of water
BFE: Effective bound fluid
CBFT2cut: Clay bound water cutoff
COPO_ob: Overburden core porosity
DPHI: Density porosity
DRT: Discrete rock type
EFZI: Equivalent flow zone indicator
FFI: Free fluid index
FZI: The flow zone indicator
FWL: Free water level
HAFWL: Height above free water level
HFU: Hydraulic flow unit
J: Leveret-J function
k: Plug permeability
K: Kaolinite
POTA-Feldspars: Potassium feldspar
NMR: Nuclear magnetic resonance
mSS: Meters below subsea level
(m): Archie cementation exponent
(n): Archie saturation exponent
Pc: Capillary pressure
PHIE: Effective porosity
$PHIE_{NMR}$*:* Effective porosity from NMR interpretation
PHIT: Total porosity
PP: Primary porosity
QO: Quartz overgrowth
SP: Secondary porosity
RESD: Deep resistivity
RESM: Shallow resistivity
RESS: Micro-resistivity
RRT: Reservoir rock type

SCAL: Special core analysis
SHM: Saturation height modeling
SWI: Irreducible water saturation
Swi_{NMR}*:* Irreducible Water Saturation calculated from NMR interpretation
SW_Ht: Saturation height modeled water saturation
T2 CUTOFF: Free fluid cutoff
T2-Dist: T2 Distribution log from the nuclear magnetic resonance tool
ϕ*:* The formation porosity
ϕ_z*:* The normalized core porosity
ρ_{ma}*:* Matrix density
ρ_{fl}*:* Fluid density
ρ_b*:* Bulk density log
ρ_{oil}*:* Oil density
ρ_{Water}*:* Water density
σ*:* Interfacial Tension
θ*:* Contact angle
k: Formation permeability